Transactions on Machine Intelligence 1(3) (2018) 115-129

ISSN Online: 2821-1693

Transactions on Machine Intelligence

Journal Homepage: https://tmachineintelligence.ir/index.php/TMI

Robust Control of Induction Motor Drives Using Prediction and Estimation of DC Link Capacitor Voltage

H. Valiyan Holagh[1,*]

[1] Master of Science, School of Electrical and Computer Engineering, University of Tehran, Tehran, Iran

ARTICLE INFO

Article History:
Received 3 June 2018
Received in revised form 20 July 2018
Accepted 9 September 2018
Available online 23 September 2018

Keywords:
Induction Motor Drives, DC Link Capacitor Voltage Fluctuations, Robust Control of Frequency Inverters

ABSTRACT

This study presents a modified control method for induction motor drives powered by a three-phase four-switch inverter. The objective is to enhance the robustness of inverters in controlling induction motors by replacing the six-switch inverter with a four-switch inverter equipped with a DC link capacitor, due to the absence of one of the legs. A novel switching method is introduced based on minimizing the effects of the capacitor voltage on the system. The switching method in the four-switch inverter is similar to space vector modulation, with the difference that the selection of active vectors and the adjustment of switching times are performed in such a way that, in addition to tracking the reference voltage, the impact of capacitor voltage fluctuations on the system is reduced. This enhances the capability of the motor and inverter under atypical operating conditions. The result of refining the switching methods is a reduction in flux and torque ripples and improved inverter performance. To evaluate and validate the proposed method, simulation results in the MATLAB environment are presented.

1. INTRODUCTION

In recent years, fault-tolerant systems with structural variability have garnered significant attention. In essence, a fault-tolerant control system consists of two subsystems: a fault detection and isolation subsystem, and a subsystem capable of structural changes in response to faults [1-5]. The primary goal of designing a fault-tolerant control system is to maintain process continuity with optimal efficiency and increased reliability in the event of faults or failures. The reliability of industrial electronics systems has always been a topic of discussion in industry, commerce, aerospace, and military applications [6].

The fault isolation unit forces the damaged switches to electrically disconnect from the system so that a new structure or configuration can be activated [7-10]. For three-phase converters, three common fault-tolerant topologies with switches for motor applications are shown in [11]. One of these topologies connects the faulty phase to the midpoint of the DC link using triacs [12, 13]. The idea of four-switch inverters for fault-tolerant control in critical and sensitive applications such as railways is highly efficient [14, 15].

* Corresponding Author: h.valiyan.h@ut.ac.ir
Master of Science, School of Electrical and Computer Engineering, University of Tehran, Tehran, Iran

http://dx.doi.org/10.47176/TMI.2018.115

Today, among various modulation techniques and methods, space vector voltage modulation is very popular. These techniques include four segments for $\pi/2$ symmetry modulation. The harmonic effects analysis in four-switch inverters is discussed in [16]. In [17], a modulation method based on space vector decomposition using $\pi/3$ symmetry, similar to six-switch inverters, is presented. References [18-21] propose simpler and more practical methods for implementing space vector modulation for four-switch inverters. Four-switch inverters have the following disadvantages compared to six-switch inverters:

- The voltage utilization factor of four-switch inverters is half that of six-switch inverters.

- The neutral point voltage of the two capacitors fluctuates.

- Unbalanced motor currents cause inverter failure and torque ripples.

Various methods have been proposed to eliminate the effects of neutral point fluctuations of the two capacitors:

1. An adaptive space vector modulation method to compensate for DC link voltage ripples in four-switch inverters is presented in [22].

2. Kim et al. investigated the motor current imbalance from the perspective of source impedance and voltage variations, which depend on the current flowing into the capacitors, and proposed a method for compensating current distortion [23].

3. Lee et al. proposed a compensation method by adjusting the switching times considering capacitor neutral point fluctuations [24].

4. Wang et al. analyzed the cause and effect of neutral point voltage fluctuations of the two capacitors from an analytical standpoint [25].

Research in this area has primarily focused on balancing the three-phase currents of four-switch inverters. Methods have also been proposed for controlling the flux and electromagnetic torque of induction motors powered by four-switch inverters. Kashif et al. [26] used a three-layer artificial neural network to control flux in induction motors powered by four-switch inverters. In [27], classical direct flux and torque control is employed. These methods assume constant capacitor voltage. In [28-30], predictive control is used to control flux and torque as well as capacitor neutral point voltage fluctuations simultaneously [31].

Each of the mentioned methods has addressed the reduction of flux and torque ripples, current distortion, and the impact of capacitor voltage fluctuations to varying degrees of success. The method presented in this paper focuses on reducing capacitor voltage fluctuations on the system, which not only reduces flux and torque ripples and current distortion but also enhances the robustness of the inverter in the new structure. The implementation of this method is based on separating the capacitor voltage fluctuations and the capacitor voltage offset. Initially, capacitor voltage fluctuations are calculated using motor current prediction, and the capacitor voltage offset is computed using an observer. Subsequently, a control algorithm based on space vector modulation is proposed for the four-switch inverter to improve inverter and motor performance.

2. REQUIREMENTS OF THE STUDY

2.1. Space Vector Modulation for Three-Phase Four-Switch Inverter

The figure below shows the structure of a four-switch inverter connected to an induction motor with an ideal DC source. In this structure, only four switches are used for switching, resulting in the creation of only four active space vectors for generating the inverter's output voltage. The switching states of these four space vectors are illustrated in Figure 1.

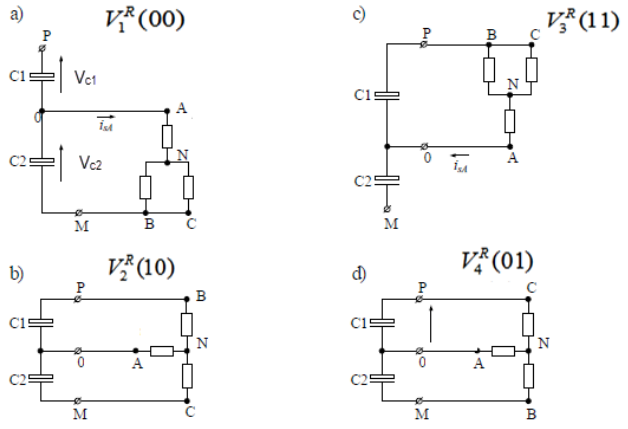

Fig. 1. Possible switching states in the secondary structure.

In Figure 1, V_{AN} V_{BN} and V_{CN} represent the phase voltages. The space voltage vectors of the inverter, V_1^R to V_4^R are calculated using Equation (1). The results of these calculations are shown in Table 1.

$$V^F = \frac{2}{3}\left(V_{AN} + e^{\frac{i2\pi}{3}} V_{BN} + e^{-\frac{i2\pi}{3}} V_{CN}\right) \tag{1}$$

Table 1. Voltage vectors related to the secondary structure of the inverter.

	Voltage Vectors
Vector Name	**Voltage Value in the Complex Plane α_β**
(00)V_1^R	$\frac{2}{3}V_{c2}$
(10)$\boldsymbol{V_2^R}$	$\frac{1}{3}(V_{c2}-V_{c1}) + j\frac{\sqrt{3}}{3}(V_{c2}+V_{c1})$
(11)$\boldsymbol{V_3^R}$	$-\frac{2}{3}V_{c1}$
(01)$\boldsymbol{V_4^R}$	$\frac{1}{3}(V_{c2}-V_{c1}) - j\frac{\sqrt{3}}{3}(V_{c2}+V_{c1})$

According to the space vector technique, the reference vector desired by the controller is obtained through the four active vectors using Equation (2):

$$V_r T_s = V_1^R t_1 + V_2^R t_2 + V_3^R t_3 + V_4^R t_4 \tag{2}$$

In the above equation, the time weights t_1 ،t_2 ،t_3 and t_4 are constrained by Equation (3):

$$T_s = t_1 + t_2 + t_3 + t_4 \tag{3}$$

To calculate the time weights, one method is to use the zero-vector distribution factor k by two pairs of odd and even vectors [19]. The time weights $|t_{13}|$ and $|t_{24}|$ are the minimum time intervals for generating the reference voltage. The remaining time interval should generate the zero vector. This amount of time is calculated using Equation (4):

$$\delta_T = T_s - |t_{13}| - |t_{24}| \tag{4}$$

Thus, the time interval $\delta_T$is divided between the two pairs of odd and even vectors according to the distribution factor k. Using the zero-vector distribution factor, the calculation of time weightst_1 ،t_2 ،t_3 and t_4 in each of the four regions is shown in Table 2.

Table 2. Switching times for the four-switch inverter in all four regions [19].

1st Region	$t_{13} > 0\,, t_{24} \geq 0$	$t_1 = t_{13} + \frac{k}{2}\delta_T\,; t_2 = t_{24} + \frac{1-k}{2}\delta_T$ $t_3 = \frac{k}{2}\delta_T\,; t_4 = \frac{1-k}{2}\delta_T$
2nd Region	$t_{13} \leq 0\,, t_{24} > 0$	$t_1 = \frac{k}{2}\delta_T\,; t_2 = t_{24} + \frac{1-k}{2}\delta_T$ $t_3 = -t_{13} + \frac{k}{2}\delta_T\,; t_4 = \frac{1-k}{2}\delta_T$
3rd Region	$t_{13} < 0\,, t_{24} \leq 0$	$t_1 = \frac{k}{2}\delta_T\,; t_2 = \frac{1-k}{2}\delta_T$ $t_3 = -t_{13} + \frac{k}{2}\delta_T; t_4 = -t_{24} + \frac{1-k}{2}\delta_T$
4th Region	$t_{13} \geq 0\,, t_{24} < 0$	$t_1 = t_{13} + \frac{k}{2}\delta_T\,; t_2 = \frac{1-k}{2}\delta_T$ $t_3 = \frac{k}{2}\delta_T\,; t_4 = -t_{24} + \frac{1-k}{2}\delta_T$

If k is set to zero, only the three vectors V_2^R ، V_4^R and V_1^R or V_3^R are used to generate the reference voltage. If k is set to one, the three vectors V_1^R ، V_3^R and V_2^R or V_4^R are used to generate the reference voltage. In this type of inverter, both stated conditions can be used simultaneously to generate the reference voltage, and even for each switching region, only one of the stated conditions can be used.

2.2. Investigation of the Impact of DC Link Capacitor Voltage Variations on the Performance of a Four-Switch Inverter

In the newly proposed structure, instead of the missing leg, two DC link capacitors with equal capacitance are added to the system. These additional capacitors first alter the system dynamics and, secondly, variations in the voltages of these capacitors cause disturbances in the inverter's performance.

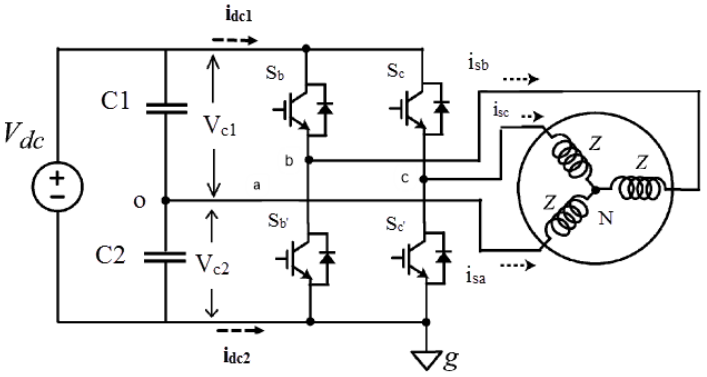

Fig. 2. Structure of the Four-Switch Inverter Connected to an Induction Motor with an Ideal DC Source

The DC link current, denoted as i_{dc1}, based on the switching states of the b and c legs and the motor currents, is expressed as follows:

$$i_{dc1} = s_b i_{sb} + s_c i_{sc} \tag{5}$$

If the Fourier transform of the DC link current is considered, given that the switching states and motor currents in Equation (5) are multiplied, it is defined in the frequency domain as the convolution between the switching states and motor current:

$$I_{dc1}(\omega) = \sum_{i=b,c} \int_{-\infty}^{+\infty} s_i(\tau) I_{si}(\omega - \tau)\, d\tau \tag{6}$$

If the modulated voltage waveform through switching for the two healthy phases is represented as in Equation (7), and the power factor $\emptyset$ is defined, the voltages of the two phases and the three-phase currents, without considering the DC link capacitors, are defined as follows:

$$V_{bo} = Mcos(\omega_o t)\ ,\quad V_{co} = Mcos\left(\omega_o t - {}^{\pi}/_{3}\right) \tag{7}$$

$$\begin{aligned} i_{sa} &= Icos(\omega_o t + \emptyset + {}^{5\pi}/_{6}) \\ i_{sb} &= Icos(\omega_o t + \emptyset + {}^{\pi}/_{6}) \\ i_{sc} &= Icos(\omega_o t + \emptyset - {}^{\pi}/_{2}) \end{aligned} \tag{8}$$

Then, by transforming the DC link current from the frequency domain to the time domain, we have:

$$i_{dc1}(t) = \frac{\sqrt{3}}{4} MIcos(\emptyset) + \frac{1}{2} I\ cos\left(\omega_o t + \emptyset + {}^{\pi}/_{6}\right) + harmonic@f_{sw}, 2f_{sw}, \ldots \tag{9}$$

From Equation (9), it can be concluded that the DC link current includes a DC component, a fundamental frequency component, and harmonic sidebands and switching frequency components. By neglecting the first and second parts of i_{dc1}in Equation (9), the voltage of the DC link capacitor can be calculated using the second part of the i_{dc1}current [25].

$$\begin{aligned} V_{c1}(t) &= V_{c1}(0) + \frac{1}{2C1}\int_0^t i_{sa}\, dt \\ &= V_{c1}(0) + \frac{I}{2\omega_o C1} \times \left[sin\left(\omega_o t + \emptyset + {}^{\pi}/_{6}\right) - sin\left(\emptyset + {}^{5\pi}/_{6}\right)\right] \end{aligned} \tag{10}$$

where $V_{c1}(0)$ is the initial voltage of capacitor C1. The second part of Equation (10) includes a sinusoidal term with an amplitude of $I/2\omega_o C1$ and a DC offset. The DC offset is determined by the initial phase angle of i_{sa}. With the variation of the capacitor voltages, the maximum voltage that the inverter can produce is reduced.

$$V_{s\,max} = \frac{1}{\sqrt{3}}.min(V_{c1}, V_{c2}) \tag{11}$$

3. PROPOSED METHODS TO MITIGATE THE IMPACT OF CAPACITOR VOLTAGE VARIATIONS ON THE INVERTER OUTPUT VOLTAGE

Analytical relations of capacitor currents show the presence of a sinusoidal term that undoubtedly causes oscillations in the voltages of the two DC link capacitors. These oscillations cause deviations in the active voltages produced in the inverter. Figure 3 illustrates the voltage deviation in the four-switch inverter due to the voltage difference between the two capacitors.

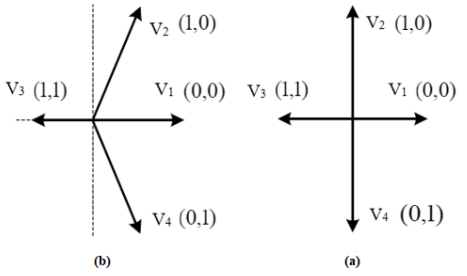

Fig. 3. Active Voltage Vectors (a) Ideal Condition $V_{c1} = V_{c2}$ (b) Condition $V_{c1} < V_{c2}$

If the inverter operates in the condition $\boldsymbol{V_{c1} < V_{c2}}$, then $\boldsymbol{V_1}$ will be larger than $\boldsymbol{V_3}$. Now, if the switching is done using the previous method, due to the change in the magnitude and amplitude of the active voltages, the inverter will not be able to produce the desired voltage. Figure 4 shows that with the variation of the capacitor voltages, the output voltage of the inverter changes undesirably.

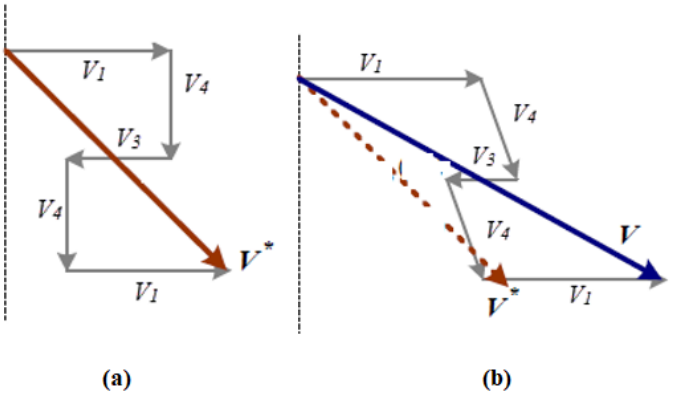

Fig. 4. Reference Voltage Generation (a) in Ideal Condition (b) in Condition $V_{c1} < V_{c2}$

Voltage imbalance or variations in the DC link capacitor voltage are represented by ΔV ccordingly, the capacitor voltages are expressed as follows:

$$\begin{aligned} &V_{c1} = \frac{V_{dc}}{2} + \Delta V \quad , \quad V_{c2} = \frac{V_{dc}}{2} - \Delta V \\ &V_{c1} + V_{c2} = V_{dc} \\ &\Delta V = \widetilde{\Delta V} + \overline{\Delta V} \end{aligned} \tag{12}$$

In the above equation, $\widetilde{\Delta V}$ represents the oscillations of the capacitor voltage, and $\overline{\Delta V}$ is the DC offset of the capacitors' voltage. The phase voltages relative to the neutral point of the motor, based on the switching states and capacitor voltages, are given by:

$$\begin{aligned} V_{aN} &= \frac{V_{c1}}{3}(-S_b - S_c) + \frac{V_{c2}}{3}(2 - S_b - S_c) \\ V_{bN} &= \frac{V_{c1}}{3}(2S_b - S_c) + \frac{V_{c2}}{3}(2S_b - S_c - 1) \\ V_{cN} &= \frac{V_{c1}}{3}(2S_c - S_b) + \frac{V_{c2}}{3}(2S_c - S_b - 1) \end{aligned} \tag{13}$$

Applying the Park transformation to the three-phase motor voltages results in:

$$\begin{bmatrix} V_{\alpha s} \\ V_{\beta s} \end{bmatrix} = \frac{2}{3}\begin{bmatrix} 1 & -0.5 & -0.5 \\ 0 & \sqrt{3}/2 & -\sqrt{3}/2 \end{bmatrix}\begin{bmatrix} V_{aN} \\ V_{bN} \\ V_{cN} \end{bmatrix} \tag{14}$$

The voltages applied to the motor in the αβ coordinate system, based on the switching states, are expressed as:

$$\begin{aligned} V_{\alpha s} &= \frac{V_{c1}}{3}(-S_b - S_c) + \frac{V_{c2}}{3}(2 - S_b - S_c) \\ V_{\beta s} &= \frac{\sqrt{3}}{2}\left[\frac{V_{c1}}{3}(S_b - S_c) + \frac{V_{c2}}{3}(S_b - S_c)\right] \end{aligned} \tag{15}$$

Substituting Equation (12) into the above relation, the inverter output voltages based on the switching states and capacitor voltage variations are obtained as:

$$\begin{aligned} V_{\alpha s} &= \frac{V_{dc}}{3}(1 - S_b - S_c) - \frac{2}{3}\Delta V \\ V_{\beta s} &= \frac{\sqrt{3}}{2} \times \frac{V_{dc}}{3}(S_b - S_c) \end{aligned} \tag{16}$$

Considering the above relation in producing the output voltage, if the controller selects each of the active voltages, the impact of capacitor voltage is observed only on the real axis. It is noteworthy that the imaginary axis includes vectors V_2 variations and V_4, while the real axis includes vectors V_1 ، V_3 and ΔV.

3.1. Adjusting Switching Times Based on DC Link Capacitor Oscillations

The switching time is calculated based on Ts. Therefore, the vector ΔV is placed on the real axis for the duration of Ts. Figure 5 shows the impact of ΔV on the active vectors. If this impact is separated from the active vectors, the magnitude and direction of the active vectors will be obtained similar to the ideal state.

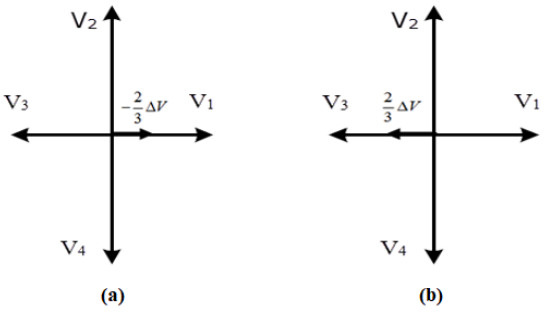

Fig. 5. Space Vectors in the Four-Switch Inverter with Vector ΔV (a) Condition $V_{c1} < V_{c2}$(b) Condition $V_{c1} > V_{c2}$

To eliminate ΔV, it is sufficient to calculate the impact of capacitor voltage variations over the duration Ts and mitigate it by adjusting the switching times of the two odd vectors that are assumed ideal. Consequently, the compensation method is formulated as follows:

$$\frac{V_{dc}}{3} \times t^* = \int_t^{t+T_s} -\frac{2}{3}\Delta V \, dt \tag{17}$$

In the above equation, t* is the required time for correcting vectors V_1 and V_3:

$$t_1^* = t_1 - \frac{t^*}{2}$$
$$t_3^* = t_3 + \frac{t^*}{2} \tag{18}$$

To obtain t*, considering that T_s is very small compared to the motor operating frequency, the integral is calculated using the trapezoidal method:

$$t^* = -\frac{\Delta V(t) + \Delta V(t+T_s)}{V_{dc}} T_s \tag{19}$$

For calculating the voltage variations at $t + T_s$using Equation (10), $\Delta V(t + T_s)$is estimated as follows:

$$\Delta V(t) = \frac{1}{2}(V_{c1}(t) - V_{c2}(t))$$
$$\Delta V(t+T_s) = \tfrac{1}{2}(V_{c1}(t+T_s) - V_{c2}(t+T_s)) = \tag{20}$$
$$\Delta V(t) + \frac{T_s i_{sa}}{2c1}$$

The final relation for t* will be:

$$t^* = -\left[\frac{2\Delta V(t)}{V_{dc}} + \frac{T_s i_{sa}}{2c1 V_{dc}}\right] T_s \tag{21}$$

As observed in the final equation, the stator current, DC link voltage, sampling time of the capacitor voltage, and the capacitor values impact the adjustment of the switching times. Therefore, it can be concluded that by changing any of the stated parameters, the proposed method can compensate for the applied changes to the circuit by controlling the switching times. The practical limitation for implementing the proposed method is that the calculated

t* should not exceed a certain threshold; in other words, the corrective time should not be greater than t^*_{max}.t^*_{max} is calculated based on the values of t_1 and t_3, and with motor operation, this threshold changes as follows:

$$t^*_{max} = \begin{cases} t_3, & t^* < 0 \\ t_1, & t^* \geq 0 \end{cases} \tag{22}$$

3.2. Control of the DC Link Capacitor Voltage Offset

Switching states for even space vectors V_2 and V_4 do not affect the capacitor voltages, whereas only the switching states of the odd vectors V_1 and V_3 are influential. Figure 6 shows these two conditions:

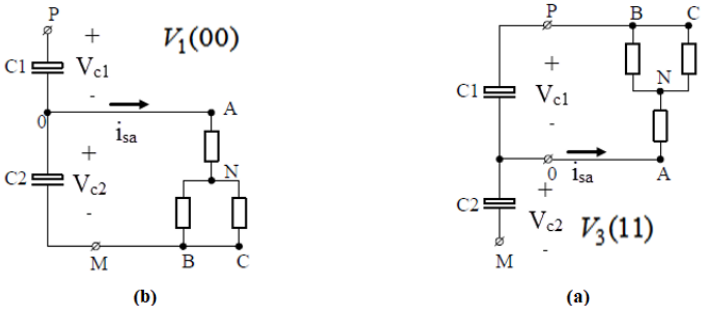

Fig. 6. Equivalent Inverter Load Structure in Switching States (a) V_3 (b) V_1

The causes of the capacitor voltage offset include: 1) the initial phase angle of i_{sa}, 2) the flow of unbalanced current to the two capacitors, 3) a significant difference between the duration of the switching states of vectors V_1 and V_3 constantly, 4) the capacitors' capacitance being smaller than a reasonable value. Given these points, calculating the offset is not straightforward. Therefore, an observer was used to extract the DC component of the capacitor voltage. The capacitor voltage observer can calculate the DC component of a signal without compromising the control dynamics, while using a low-pass filter to eliminate low-frequency oscillations imposes a significant delay on the control system. Utilizing the observer to extract the DC component of the capacitor voltage allows the voltage control to eliminate the offset more quickly. Moreover, because low-frequency oscillations are completely separated from the capacitor voltage offset control loop, the control loop's bandwidth is significantly increased. To design the DC link voltage observer for capacitor C1, we have:

$$\begin{cases} \dot{e}_1 = \omega_s\left(e_2 + \tilde{V}_{DC}\right) - \gamma_1 e_1 \\ \dot{e}_2 = -\omega_s e_2 - \gamma_2 e_1 \\ \tilde{V}_{DC} = -\mu\omega_s e_1 \end{cases} \tag{23}$$

Offset control in capacitor voltage is managed using the zero-vector distribution factor and the sign of the current entering the capacitors. The switching method remains stable at k = 1 due to the lower distortion in motor currents under steady-state conditions. To generate a zero vector, two collinear vectors are used. The zero-vector distribution factor (k) is employed to determine which two collinear vectors to use. Since the switching times influence the charging and discharging of capacitors within a cycle, this vector is utilized to eliminate the offset voltage in the capacitors. Depending on the polarity of the current passing through the capacitors, k is adjusted to either increase or decrease the charging and discharging. As illustrated in Figure 6, if $\overline{\Delta V}$ is positive, i_{sa} current passing through two capacitors is used to reduce or eliminate it. If i_{sa} is positive, to reduce $\overline{\Delta V}$ the time using vectors V_1 and V_3 is decreased (k=0), and if i_{sa} is negative, the time using vectors V_1 and $V_3$is increased (k=1). Conversely, if $\overline{\Delta V}$ is negative, to increase or eliminate it, if i_{sa} is positive, the time using vectors V_1 and V_3 is increased (k=1), and if i_{sa} is negative, the time using vectors V_1 and V_3 is decreased (k=0).

4. SIMULATION RESULTS

To simulate and verify the stated relationships, a three-phase squirrel cage induction motor with nominal specifications of 3 kW, 380 volts, and 1415 rpm was used.

4.1. Simulation of Reducing the Effect of Capacitor Voltage Fluctuations on the System

Capacitor voltage fluctuations encompass the AC component of the capacitor voltage variations, with the amplitude of these fluctuations related to motor operation. Due to the inverter structure, these fluctuations cannot be eliminated, but their effect on the inverter output can be reduced by controlling switching times. Current waveforms, electric torque, stator flux, and capacitor voltages are shown in Figures 7, 8, 9, and 10, respectively. The method to reduce capacitor voltage fluctuations by adjusting switching times is applied at t = 1s. In Figure 7, it is observed that after correcting the switching times, current imbalance is eliminated, but total harmonic distortion in the stator current remains. Balancing the currents through switching time correction alone improves the electric torque and flux of the induction motor. The reduction in torque ripple and stator flux ripple is shown in Figures 8 and 9, respectively.

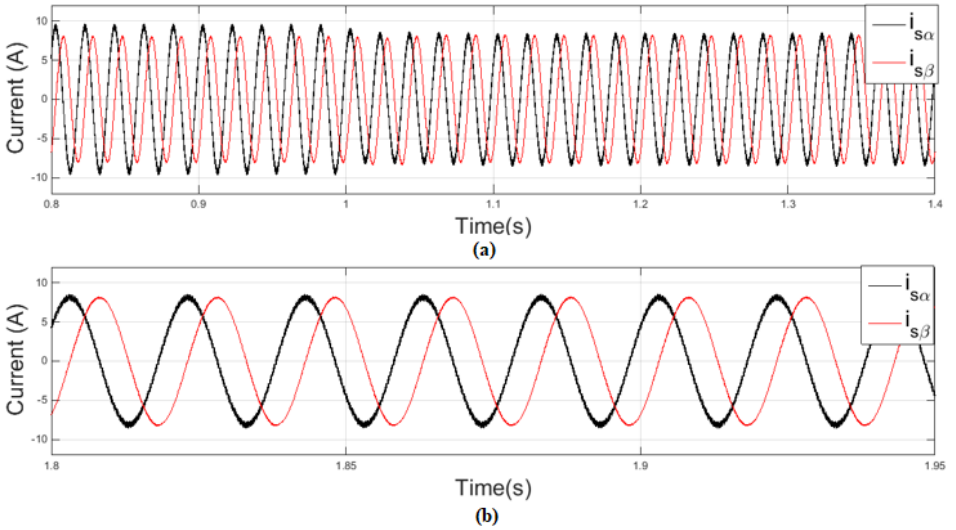

Fig.7. Stator current waveform a) before and after switching time correction b) after switching time correction.

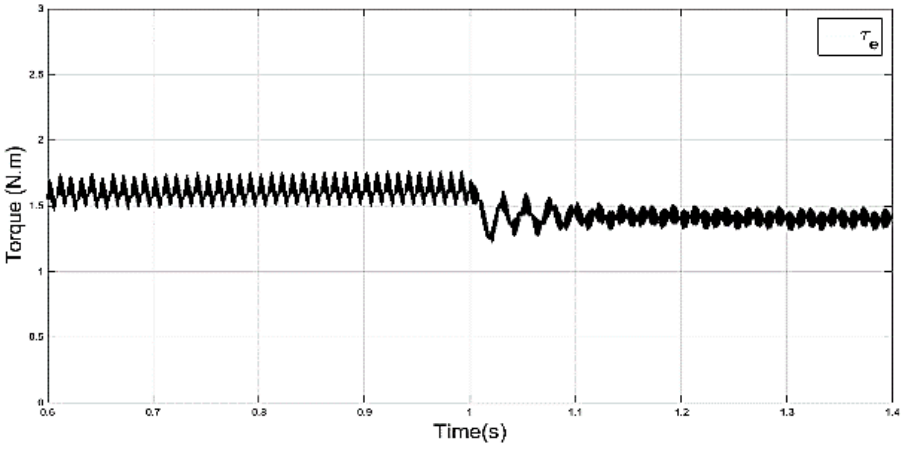

Fig. 8. Electric torque waveform, before and after switching time correction.

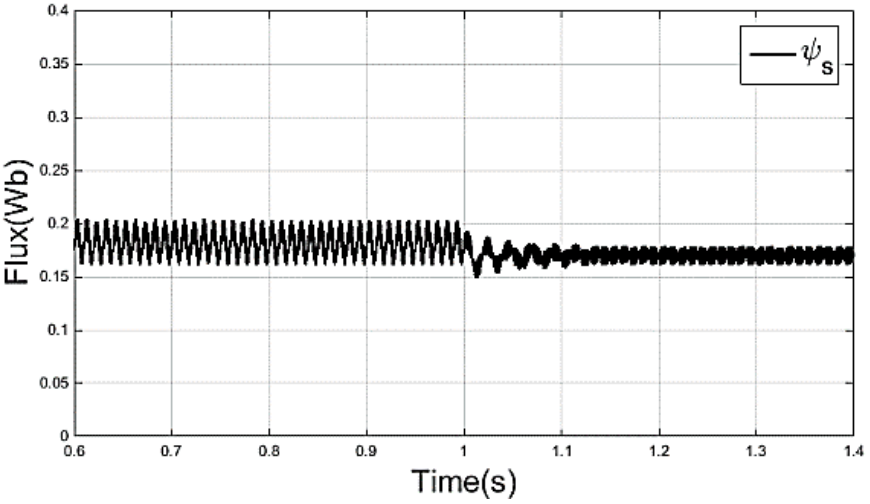

Fig. 9. Stator flux amplitude waveform, before and after switching time correction.

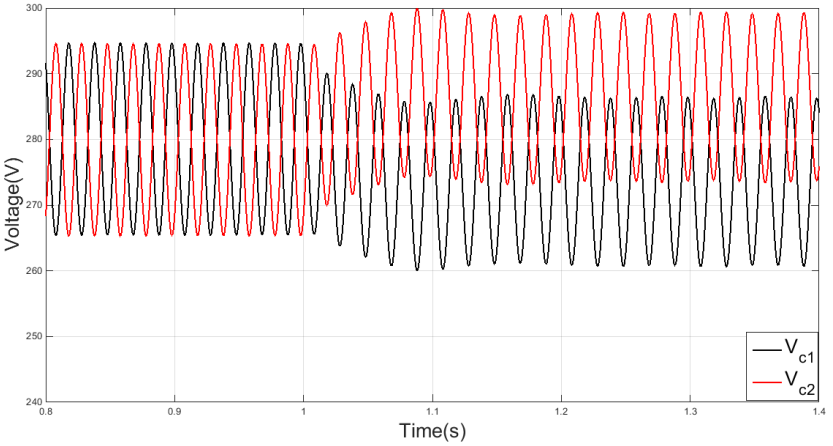

Fig. 10. Capacitor voltage waveform, before and after switching time correction.

In Figure 10, it is observed that since the switching time correction, DC link capacitor voltage fluctuations have increased. The additional fluctuations consist only of the DC offset, which is due to switching time adjustments. Fortunately, the offset on the inverter output voltage can be controlled by selecting appropriate voltage vectors.

4.2. Simulation of Capacitor Voltage Offset Control Using an Observer

The waveforms of capacitor voltage, estimated DC voltage, and stator current are shown in Figures 11, 12, and 13, respectively. Offset control of capacitor voltage through switching time correction is applied at t = 1s. This section also uses the proposed method to reduce the effect of capacitor fluctuations on the output voltage. By applying the proposed offset control method at t = 1s, as seen in the capacitor voltage waveform in Figure 11, the created offset in the capacitor voltage is effectively eliminated. Moreover, in Figure 12, it is observed that the DC voltage of the capacitor is estimated very quickly.

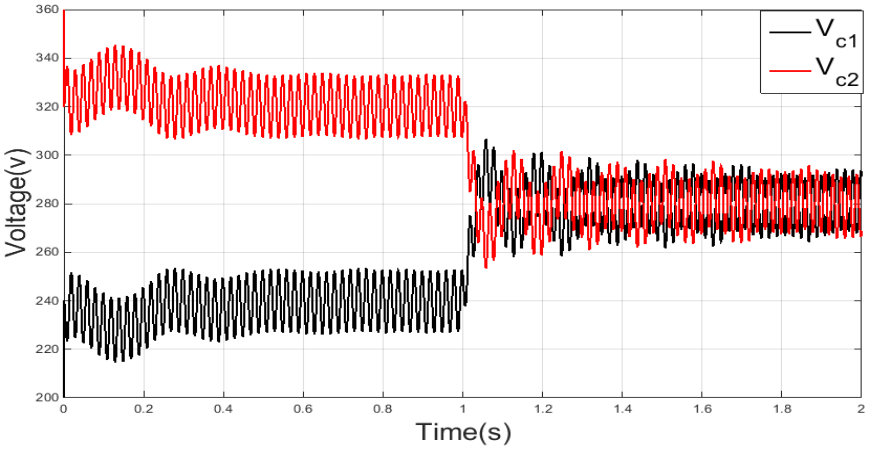

Fig. 11. Capacitor voltage waveform, before and after capacitor voltage offset control.

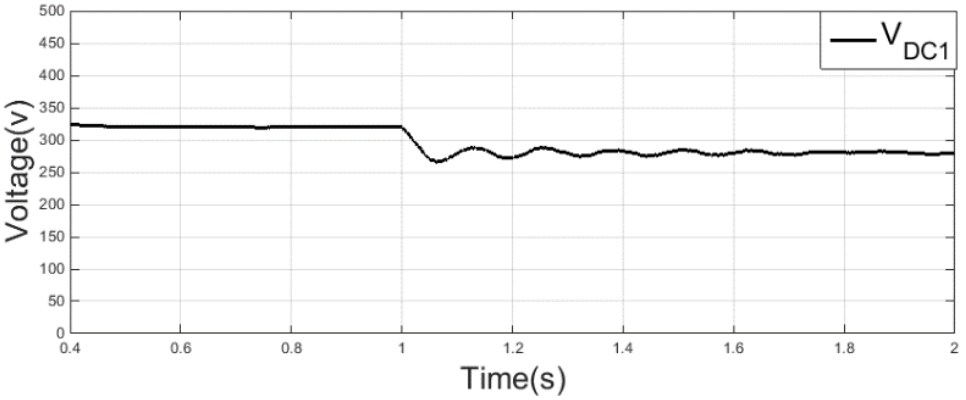

Fig. 12. Estimated DC voltage waveform using an observer.

As shown in Figure 13, current imbalance is absent before offset control due to the offset in capacitor voltage. The primary reason for the absence of current imbalance is that switching time corrections are used to reduce the effect of voltage fluctuations. Thus, switching time corrections can eliminate current imbalance despite the capacitor voltage offset. This result is maintained after offset control as well. Balancing currents through switching time correction with the presence of capacitor voltage offset control improves the electric torque and flux of the induction motor.

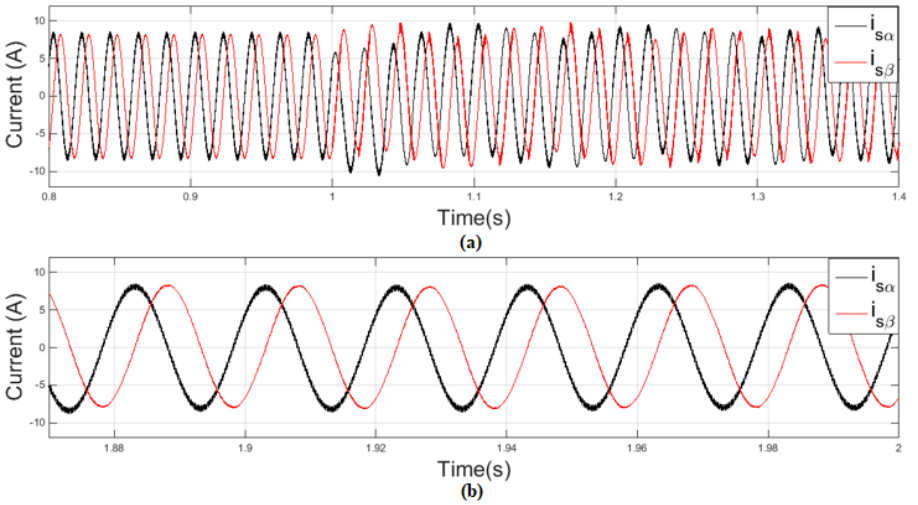

Fig. 13. Stator current waveform a) before and after capacitor voltage offset control b) after capacitor voltage offset control.

5. CONCLUSION

The added DC link capacitors in the inverter and motor structure alter the system dynamics, and the created voltage changes in the capacitors degrade the performance of the inverter and motor. The derived relationship for capacitor voltage shows that the changes consist of a sinusoidal term with amplitude $I/2\omega_o C1$ and a DC offset term. Initially, the amplitude of capacitor voltage fluctuations and a method to reduce their effect on the inverter output voltage were calculated. Then, the switching times were computed based on capacitor fluctuations. The changes in capacitor voltage over the period Ts (cycle period) were calculated by predicting the capacitor voltage at t + Ts, and the necessary time for correcting odd vectors was obtained. In the second part of the paper, DC link capacitor voltage offset control was addressed. Given that analytically calculating the offset value is not feasible, an observer was used to extract the capacitor voltage offset. The observer can calculate the DC component of a signal without compromising control dynamics. With the offset voltage in hand, an algorithm was proposed for controlling the capacitor voltage offset based on the zero-vector distribution factor and the polarity of the current entering the capacitors.

Transparency Statement

The data supporting this study are available upon reasonable request to the corresponding author, subject to ethical and confidentiality considerations.

Acknowledgments

We would like to express our gratitude to all individuals who contributed to this project.

Declaration of Interest

The authors declare that they have no competing interests.

Funding

This research received no specific grant from any funding agency, commercial, or not-for-profit sectors.

REFERENCES

[1] Yang, H., Jiang, X., Li, B., Yang, H. J., Miller, M. A., Yang, A., Dhar, A., & Pavletich, N. (2017). Structural mechanisms of mTORC1 activation by RHEB and inhibition by PRAS40. Nature, 552, 368-373. https://doi.org/10.1038/nature25023

[2] Banerjee, T., Gottschling, K., Savasci, G., Ochsenfeld, C., & Lotsch, B. (2018). H2 evolution with covalent organic framework photocatalysts. ACS Energy Letters, 3, 400-409. https://doi.org/10.1021/acsenergylett.7b01123

[3] Zidan, A., Khairalla, M., Abdrabou, A., Khalifa, T., Shaban, K., Abdrabou, A., Shatshat, R., & Gaouda, A. (2017). Fault detection, isolation, and service restoration in distribution systems: State-of-the-art and future trends. IEEE Transactions on Smart Grid, 8, 2170-2185. https://doi.org/10.1109/TSG.2016.2517620

[4] Worthy, A., Grosjean, A., Pfrunder, M. C., Xu, Y., Yan, C., Edwards, G., Clegg, J., & McMurtrie, J. C. (2018). Atomic resolution of structural changes in elastic crystals of copper(II) acetylacetonate. Nature Chemistry, 10(1), 65-69. https://doi.org/10.1038/nchem.2848

[5] Jousset, P., Reinsch, T., Ryberg, T., Blanck, H., Clarke, A., Aghayev, R., Hersir, G., Henninges, J., Weber, M., & Krawczyk, C. (2018). Dynamic strain determination using fibre-optic cables allows imaging of seismological and structural features. Nature Communications, 9. https://doi.org/10.1038/s41467-018-04860-y

[6] Kastha, D., & Bose, B. K. (1994). Investigation of fault modes of voltage-fed inverter system for induction motor drive. IEEE Transactions on Industry Applications, 30(4), 1028-1038. https://doi.org/10.1109/28.297920

[7] Bolognani, S., Zordan, M., & Zigliotto, M. (2000). Experimental fault-tolerant control of a PMSM drive. IEEE Transactions on Industrial Electronics, 47(5), 1134-1141. https://doi.org/10.1109/41.873223

[8] de Araujo Ribeiro, R. L., Jacobina, C. B., Da Silva, E. R. C., & Lima, A. M. N. (2004). Fault-tolerant voltage-fed PWM inverter AC motor drive systems. IEEE Transactions on Industrial Electronics, 51(2), 439-446. https://doi.org/10.1109/TIE.2004.825284

[9] Song, Y., & Wang, B. (2013). Analysis and experimental verification of a fault-tolerant HEV powertrain. IEEE Transactions on Power Electronics, 28(12), 5854-5864. https://doi.org/10.1109/TPEL.2013.2245513

[10] Zhang, W., Xu, D., Enjeti, P. N., Li, H., Hawke, J. T., & Krishnamoorthy, H. S. (2014). Survey on fault-tolerant techniques for power electronic converters. IEEE Transactions on Power Electronics, 29(12), 6319-6331. https://doi.org/10.1109/TPEL.2014.2304561

[11] Hoang, K., Zhu, Z. Q., Foster, M. P., & Stone, D. A. (2010). Comparative study of current vector control performance of alternate fault tolerant inverter topologies for three-phase PM brushless ac machine with one phase open-circuit fault. In Power Electronics, Machines and Drives (PEMD 2010), 5th IET International Conference on (pp. 1-6). IET. https://doi.org/10.1049/cp.2010.0052

[12] Campos-Delgado, D., Espinoza-Trejo, D., & Palacios, E. (2008). Fault-tolerant control in variable speed drives: A survey. IET Electric Power Applications, 2(2), 121-134. https://doi.org/10.1049/iet-epa:20070203

[13] Fu, J.-R., & Lipo, T. A. (1993). A strategy to isolate the switching device fault of a current regulated motor drive. In Industry Applications Society Annual Meeting, 1993., Conference Record of the 1993 IEEE (pp. 1015-1020). IEEE.

[14] Liu, T.-H., Fu, J.-R., & Lipo, T. A. (1993). A strategy for improving reliability of field-oriented controlled induction motor drives. IEEE Transactions on Industry Applications, 29(5), 910-918.

https://doi.org/10.1109/28.245714

[15] Welchko, B. A., Lipo, T. A., Jahns, T. M., & Schulz, S. E. (2004). Fault tolerant three-phase AC motor drive topologies: A comparison of features, cost, and limitations. IEEE Transactions on Power Electronics, 19(4), 1108-1116. https://doi.org/10.1109/TPEL.2004.830074

[16] Van Der Broeck, H. W., & Skudelny, H.-C. (1988). Analytical analysis of the harmonic effects of a PWM AC drive. IEEE Transactions on Power Electronics, 3(2), 216-223. https://doi.org/10.1109/63.4352

[17] Klima, J. (2005). Time and frequency domain analysis of fault-tolerant space vector PWM VSI-fed induction motor drive. IEE Proceedings - Electric Power Applications, 152(4), 765-774. https://doi.org/10.1049/ip-epa:20045099

[18] Alavije, H. S., & Akhbari, M. (2011). Investigation of induction motor drive behavior in low-cost fault tolerant control for electric vehicles. In Power Engineering and Optimization Conference (PEOCO), 2011 5th International (pp. 176-181). IEEE.

[19] de Rossiter Correa, M. B., Jacobina, C. B., da Silva, E. R. C., & Lima, A. M. N. (2006). A general PWM strategy for four-switch three-phase inverters. IEEE Transactions on Power Electronics, 21(6), 1618-1627. https://doi.org/10.1109/TPEL.2006.882964

[20] Sobanski, P., & Orlowska-Kowalska, T. (2014). Analysis of space vector modulation technique in inverter-fed fault-tolerant induction motor drive. In Power Electronics and Motion Control Conference and Exposition (PEMC), 2014 16th International (pp. 1024-1029). IEEE. https://doi.org/10.1109/EPEPEMC.2014.6980643

[21] Li, Z., Zhang, M., Guo, Y., & Zhang, X. (2017). Overmodulation strategy for four-switch three-phase inverter based on virtual voltage vector. In Control Conference (CCC), 2017 36th Chinese (pp. 7364-7369). IEEE.

[22] Blaabjerg, F., Neacsu, D. O., & Pedersen, J. K. (1999). Adaptive SVM to compensate DC-link voltage ripple for four-switch three-phase voltage-source inverters. IEEE Transactions on Power Electronics, 14(4), 743-752. https://doi.org/10.1109/63.774214

[23] Kim, J., Hong, J., & Nam, K. (2009). A current distortion compensation scheme for four-switch inverters. IEEE Transactions on Power Electronics, 24(4), 1032-1040. https://doi.org/10.1109/TPEL.2008.2011552

[24] Lee, D.-M., Park, J.-B., & Toliyat, H. A. (2013). A simple current ripple reduction method for B4 inverters. Journal of Electrical Engineering and Technology, 8(5), 1062-1069. https://doi.org/10.5370/JEET.2013.8.5.1062

[25] Wang, R., Zhao, J., & Liu, Y. (2011). A comprehensive investigation of four-switch three-phase voltage source inverter based on double Fourier integral analysis. IEEE Transactions on Power Electronics, 26(10), 2774-2787. https://doi.org/10.1109/TPEL.2011.2119381

[26] Kashif, S. A. R., Saqib, M. A., & Zia, S. (2011). Implementing the induction-motor drive with four-switch inverter: An application of neural networks. Expert Systems with Applications, 38(9), 11137-11148. https://doi.org/10.1016/j.eswa.2011.02.159

[27] El Badsi, B., Bouzidi, B., & Masmoudi, A. (2013). DTC scheme for a four-switch inverter-fed induction motor emulating the six-switch inverter operation. IEEE Transactions on Power Electronics, 28(7), 3528-3538. https://doi.org/10.1109/TPEL.2012.2225449

[28] Sobanski, P., & Orlowska-Kowalska, T. (2015). Predictive flux and torque control of induction motor drive under post-fault operation of three-phase voltage inverter. In Industrial Technology (ICIT), 2015 IEEE International Conference on (pp. 2333-2338). IEEE. https://doi.org/10.1109/ICIT.2015.7125442

[29] Zhou, D., Zhao, J., & Liu, Y. (2015). Predictive torque control scheme for three-phase four-switch inverter-fed induction motor drives with DC-link voltages offset suppression. IEEE Transactions on Power Electronics, 30(6), 3309-3318. https://doi.org/10.1109/TPEL.2014.2338395

[30] Zhou, D., Li, X., & Tang, Y. (2018). Multiple-vector model-predictive power control of three-phase four-switch rectifiers with capacitor voltage balancing. IEEE Transactions on Power Electronics, 33(7), 5824-5835. https://doi.org/10.1109/TPEL.2017.2750766

[31] Zeng, Z., Zheng, W., & Zhao, R. (2017). Performance analysis of the zero-voltage vector distribution in three-phase four-switch converter using a space vector approach. IEEE Transactions on Power Electronics, 32(1), 260-273. https://doi.org/10.1109/TPEL.2016.2532477